Title:

Activation of ChvG-ChvI regulon by cell wall stress confers resistance to β-lactam antibiotics and initiates surface spreading in *Agrobacterium tumefaciens*

Authors:

Michelle A. Williams*[$], Jacob M. Bouchier*, Amara K. Mason, and Pamela J.B. Brown[#]

Affiliations:

Division of Biological Sciences, University of Missouri-Columbia, Columbia, Missouri, 65211

Running title: Cell wall stress activates the ChvG-ChvI pathway in *A. tumefaciens*

*denotes equal contributions

[#]Corresponding author:

brownpb@missouri.edu

(573) 884-0384

Present address:

[$]Boulevard Brewery, 2501 Southwest Blvd, Kansas City, MO 64108

ABSTRACT

A core component of nearly all bacteria, the cell wall is an ideal target for broad spectrum antibiotics. Many bacteria have evolved strategies to sense and respond to antibiotics targeting cell wall synthesis, especially in the soil where antibiotic-producing bacteria compete with one another. Here we show that cell wall stress caused by both chemical and genetic inhibition of the essential, bifunctional penicillin-binding protein PBP1a prevents microcolony formation and activates the canonical host-invasion two-component system ChvG-ChvI in *Agrobacterium tumefaciens*. Using RNA-seq, we show that depletion of PBP1a for 6 hours results in a downregulation in transcription of flagellum-dependent motility genes and an upregulation in transcription of type VI secretion and succinoglycan biosynthesis genes, a hallmark of the ChvG-ChvI regulon. Depletion of PBP1a for 16 hours, results in differential expression of many additional genes and may promote a general stress response. Remarkably, the overproduction of succinoglycan causes cell spreading and deletion of the succinoglycan biosynthesis gene *exoA* restores microcolony formation. Treatment with cefsulodin phenocopies depletion of PBP1a and we correspondingly find that *chvG* and *chvI* mutants are hypersensitive to cefsulodin. This hypersensitivity only occurs in response to treatment β-lactam antibiotics and moenomycin, suggesting that the ChvG-ChvI pathway may play a key role in resistance to antibiotics targeting cell wall synthesis. Finally, we provide evidence that ChvG-ChvI likely has a conserved role in conferring resistance to cell wall stress within the Alphaproteobacteria.

AUTHOR SUMMARY

Soil dwelling bacteria reside in changing environments requiring them to frequently adapt to stressful conditions to ensure survival. The bacterial envelope provides structural integrity and protection against osmotic stress and turgor pressure imposed by the environment. While the mechanisms of cell membrane and cell wall biogenesis have been extensively studied, our understanding of how diverse microbes respond to cell envelope and cell wall stress to increase their fitness remains limited. In this work, we identify ChvG-ChvI regulon as an envelope stress response system that confers protection under cell wall stress conditions in the bacterial plant pathogen *Agrobacterium tumefaciens*. This is a new function for the well-characterized ChvG-ChvI pathway which is also acid induced and promotes plant host invasion. Our results suggest that the ChvG-ChvI pathway has a broadly conserved role in protecting Alphaproteobacterial cells from extracellular stress and a more specific role in response to acid stress and promoting plant-microbe interactions.

INTRODUCTION

The soil environment is constantly in flux and can undergo rapid changes in hydration, nutrient availability, temperature, acidity levels and many other abiotic and biotic factors [1]. To survive in these conditions, soil-dwelling bacteria must be able to monitor and respond to the changes around them. One of the main mechanisms bacteria employ to monitor changes in their environment is coupling environmental stimuli to transcriptional regulation using two-component systems (TCS) [2]. In turn transcriptional changes can modify bacterial behavior. In the plant-pathogen *Agrobacterium tumefaciens*, two TCS sense the presence of a potential host and initiate transcription programs that transition the bacterium into a virulent state [3].

70 The VirA-VirG histidine kinase/response-regulator pair is a characteristic of
71 Agrobacteria and responds to plant phenolic compounds such as acetosyringone.
72 Activation induces expression of the *vir* regulon, which encodes genes that are required
73 for pathogenicity and plant transformation [4]. The ChvG-ChvI TCS is more broadly
74 conserved across many Alphaproteobacteria but has been best characterized among
75 the plant symbionts of Rhizobiales such as *Sinorhizobium meliloti* [5,6]. Activation of
76 ChvG-ChvI is required for the transition from a free-living bacterium to a host-associated
77 lifestyle [7].
78 In *S. meliloti* and *A. tumefaciens* ChvG-ChvI is regulated by the periplasmic
79 protein ExoR. Under neutral conditions, ExoR binds to and represses ChvG; however,
80 when cells are exposed to acidic conditions, ExoR is proteolyzed, which allows for
81 activation of the ChvG-ChvI TCS [8,9]. ChvI induces transcriptional changes in many
82 genes across several major pathways. For example, ChvI upregulates transcription of
83 *mirA,* encoding a repressor of the motility response regulator Rem and ultimately
84 resulting in suppression of genes for motility and chemotaxis [10]. ChvI also upregulates
85 genes for exopolysaccharide production and, in *A. tumefaciens,* induction of the Type VI
86 Secretion System (T6SS) [11].
87 Conservation of the ChvG-ChvI TCS is taxonomically constrained to several
88 orders of Alphaproteobacteria, many of whom have free-living lifestyles that are never
89 host-associated [6]. This begs the question: why is the ChvG-ChvI pathway conserved
90 in so many non-host-associated bacteria? Recent interest in the ChvG-ChvI pathway of
91 *Caulobacter crescentus* (ChvGI) provides a glimpse at the function of the pathway in the
92 context of a bacterium with a drastically different ecological niche to that of *A.*

93 *tumefaciens* or *S. meliloti*. ChvGI of *C. crescentus* senses and responds to osmotic
94 stress and mutants of ChvGI are sensitive to several cell-wall targeting antibiotics
95 [12,13]. It remains unclear if this function is solely a characteristic of *C. crescentus*
96 ChvGI or if it is conserved across ChvG-ChvI orthologs.

97 Although the cell wall is an essential feature of bacteria that protects them from
98 environmental stressors, relatively little is known about how bacteria sense and respond
99 to changes in the composition of their cell wall. Peptidoglycan (PG) is a heteroglycan
100 decorated with cross-linked peptide stems and is the primary component of bacterial
101 cell walls. During elongation in *A. tumefaciens*, nascent PG insertion is constrained to
102 the pole. Polar growth is a characteristic of Rhizobiales and does not require the
103 canonical MreB-RodA-PBP2 elongation complex. Indeed, all members of Rhizobiales
104 have lost this complex entirely [14,15].

105 We showed that PBP1a is essential in *A. tumefaciens* and is the primary driver of
106 polar growth. Depletion of PBP1a eliminates nascent PG insertion at the growth pole,
107 leading to shorter cells that have compositional changes in PG [16]. In addition to its
108 role in polar PG insertion, here we observe that during PBP1a depletion cells spread
109 apart rather than form microcolonies. To better understand this phenotype, we used
110 RNA-seq to obtain transcriptional profiles of cells depleted of PBP1a after 6 hours,
111 corresponding to the onset of the spreading phenotype, and after 16 hours.
112 Transcriptomic changes closely mimic the transcriptome changes seen when ChvG-
113 ChvI is activated in *A. tumefaciens*, including downregulation of genes for motility and
114 chemotaxis and upregulation of genes for exopolysaccharide biosynthesis and T6SS.

115 Here we experimentally validate the RNA-seq results, confirming the impacts of PBP1a
116 depletion on the physiology and behavior of *A. tumefaciens*.
117
118 **RESULTS**
119 **PBP1a depletion prevents proper microcolony formation**
120 Here, we grew PBP1a depleted cells on agarose pads and saw that these cells
121 exhibit surface spreading rather than forming closely packed microcolonies (Fig 1A).
122 Additionally, when centrifuging cultures of PBP1a-depleted cells, we observed that the
123 cells did not pellet (Fig S1). Considering the possibility that depletion of PBP1a
124 somehow signals for these phenomena, we decided to look at RgsM, another enzyme
125 required for polar elongation. Previous work points to RgsM activity being required for
126 incorporation of nascent PG by PBP1a [17]. However, depletion of RgsM did not cause
127 surface spreading (Fig 1A) indicating that an imbalance of PG hydrolysis and synthesis
128 triggers spreading and the inability pellet in *A. tumefaciens*. Deletions of genes
129 encoding other high molecular weight PBPs and *mtgA*, a PG transglycosylase did not
130 induce spreading (Fig 1B).
131 Timelapse microscopy revealed that after ~6 hours of PBP1a depletion cells
132 spread apart, though the movement of cell appears to be confined within a relatively
133 small region of the agarose pad (Fig 1C, Movie S1). Since spreading is confined and
134 occurs over the course of many hours, we suspected that this phenomenon was not
135 simply caused by the activation of swimming motility.
136
137 **PBP1a depletion induces global transcriptome changes**

138 To understand the spreading phenotype caused by PBP1a depletion, we
139 compared the transcriptomes of cells at the onset or late stage of the surface spreading
140 phenotype. Cells were grown with or without the inducer Isopropyl β-D-1-
141 thiogalactopyranoside (IPTG) for *mrcA,* encoding PBP1a, expression for 6 or 16 hours
142 (Fig. 2A). As a baseline, we compared transcriptional profiles of WT in the presence and
143 absence of IPTG to the PBP1a depletion strain in the presence of IPTG. The addition of
144 IPTG did not alter gene expression profiles of WT cells, and only minor differences were
145 apparent between the PBP1a depletion strain background and WT when both strains
146 are grown in the presence of IPTG (Fig S2). We next compared differences in the
147 PBP1a replete strain to the PBP1a depleted strain at either 6- or 16-hours post
148 depletion (Fig 2A). Using a p-value < 0.05 and log2 fold-change (L2FC) > 2.0, we
149 identified 91 and 306 genes that were differentially expressed in the + PBP1a strain
150 compared to the 6- or 16-hour depletion, corresponding to 2% and 6% of the total
151 genes, respectively.
152 Overall, we observed large-scale changes in a diverse and widespread range of
153 genes that are regulated in response to PBP1a depletion. Initially, the response to
154 PBP1a depletion is primarily mediated by chromosomally encoded rather than plasmid
155 encoded genes. *A. tumefaciens* has a circular chromosome, which houses roughly half
156 (51.7%) of the protein-coding genes, a linear chromosome (34.7%) and two mega
157 plasmids, the At plasmid (10%) and Ti plasmid (3.6%). Most of the genes differentially
158 expressed at both time points during PBP1a depletion were encoded on the linear and
159 circular chromosomes (Fig. 2A). Most of the differentially abundant genes from the 6-
160 hour timepoint were also present in the 16-hour timepoint. For several of these genes,

161 the magnitude of differential transcript abundance remained relatively constant. For
162 example, the response regulator ChvI, had an increased relative abundance early in
163 response to PBP1a depletion that remained constant in the 16-hour timepoint. In
164 contrast, several genes displayed a continuous increase or decrease in transcript
165 abundance between the 6- and 16-hour timepoints, including genes that encode
166 proteins necessary for assembly of flagella and type 6 secretion system machinery.
167 Finally, several genes were only differentially abundant at the 16-hour timepoint,
168 including many genes encoding proteins important for cell envelope homeostasis such
169 as the Tol-Pal system [18], and >30 ABC transporters.
170 To further categorize the diverse set of differentially abundant genes we
171 identified Clusters of Orthologous Groups (COGs) in the 16-hour timepoint and
172 classified them based on functional categories represented by a single letter code
173 (Figure 2B) [19,20]. The most affected COG category was motility (N). Decreased
174 abundance of mRNAs containing genes which encode structural flagella proteins further
175 supports the hypothesis that the spreading phenotype is independent of flagella-based
176 motility. The COG category with the largest proportion of increased differentially
177 abundant genes was cell wall, membrane, and envelope biogenesis (M). Notably, no
178 significant changes in the transcripts of other penicillin-binding proteins or
179 glycosyltransferases were observed in response to loss of PBP1a (Table S1). However,
180 significant changes in transcripts encoding cell wall remodeling enzymes such as LD-
181 transpeptidases, endopeptidases, and soluble lytic transglycosylases were detected
182 (Table S1). Atu0844, an LD-transpeptidase, was strongly downregulated suggesting it
183 may play an important role in polar growth alongside PBP1a. Additionally, one putative

184 β-lactamase gene, Atu0933, was strongly upregulated, which may provide a strategy to
185 protect against cell wall damage. In addition, many of the genes found in this COG
186 category encode cell envelope homeostasis and osmotic stress response proteins,
187 including the Tol-Pal system, several outer membrane proteins (i.e. AopB), and
188 periplasmic sensors (i.e. CreD).

189 At the 16-hour timepoint, the largest changes to cellular metabolism occurred in
190 the inorganic ion transport and metabolism (P) and amino acid metabolism and
191 transport (E) COG categories, suggesting a shift in nutrient uptake and metabolism, as
192 expected during a general stress response. Interestingly, the six most downregulated
193 genes in the 16-hour timepoint, with the exception of *mrcA*, encoding PBP1a, were *yciC*
194 (Atu3181), *zinT* (Atu1049), *troC* (Atu3180), *troB* (Atu3179), *troA* (Atu3179), and
195 Atu3184, all of which are major components of cytoplasmic zinc uptake in
196 *Agrobacterium tumefaciens* (Fig 2B, bottom) [21].

197 We also observed large increases and decreases in the transcript abundance of
198 signal transduction genes. Transcription of *exoR* (Atu1715), *chvG* (Atu0033), and *chvI*
199 (Atu0034) were upregulated at both the 6-hour (L2FC = 0.995, 1.42, and 2.18) and 16-
200 hour (L2FC = 2.20, 1.41, and 2.27) depletions of PBP1a. Transcription of genes
201 encoding three other two-component systems were also strongly upregulated (Fig S3,
202 Table S1).

203

204 **Transcriptome changes during PBP1a depletion mimic activation of the ChvG-**
205 **ChvI two-component system.**

206 Transcription of *virG*, encoding a TCS response regulator, was also strongly
207 upregulated in both the 6-hour (L2FC = 2.61) and 16-hour (L2FC = 4.02) timepoints (Fig
208 S3, Table S1). Transcription of *virG* has been reported to be upregulated under both
209 host-invasion and virulence-inducing conditions [11]. Because *virG* was also
210 upregulated during depletion of PBP1a, we reasoned that PBP1a depletion may be
211 mimicking one of these two conditions. Using comparative transcriptomics, we
212 compared the 150 most differentially expressed genes (DEGs) against published
213 datasets that simulate host-invasion conditions (Δ*exoR* & pH 5.5) and virulence-
214 inducing conditions (acetosyringone treatment & growth on AB media) [22][23]. We
215 found that L2FC values of the 6-hour PBP1a depletion RNA-seq dataset correlated with
216 the two host-invasion conditions and not with the virulence-inducing datasets, as
217 indicated by the spearmen rho correlation coefficient for each comparison (Δ*exoR*, rho =
218 0.875; pH 5.5, rho = 0.766) (Fig 3 and S4). Rho values near 1 indicate similar DEGs
219 between each dataset. Rho values near 0 would indicate no similar DEGs between
220 each dataset (Fig 3A). Interestingly, each of these two datasets have been implicated in
221 activation of the ChvG-ChvI pathway [9,11]. Correlation with each strongly implicates
222 ChvG-ChvI activation in our RNA-seq, suggesting that depletion of PBP1a may provide
223 a signal leading to similar changes described to occur during the transition to a host-
224 invasion lifestyle. While this trend was maintained in the 16-hour timepoint, we observed
225 additional genes that were differentially expressed under depletion of PBP1a, but not in
226 the Δ*exoR* and pH 5.5 datasets (Fig 3, Fig S4B). Indeed, the rho values for the 16-hour
227 depletion of PBP1a compared to the host-invasion datasets (Δ*exoR*, rho = 0.529; pH
228 5.5, rho = 0.739 were lower than the 6-hour comparisons. Additionally, we found 217

229 more genes with L2FC > 2.0 in the 16-hour depletion than in the 6-hour depletion (Fig
230 3B). Together, these findings suggest that longer depletions of PBP1a may result in the
231 activation of additional regulons beyond ChvG-ChvI.
232 Overall, a large number and variety of genes are regulated in response to
233 depletion of PBP1a. Although many of these changes in gene expression have been
234 reported previously in response to low pH or deletion of the ChvG-ChvI negative
235 regulator ExoR, these changes have never been associated with loss of a cell wall
236 synthase in *A. tumefaciens*. These observations indicate that there are additional
237 mechanisms that can activate the ChvG-ChvI TCS.
238
239 **Succinoglycan overproduction is required for cell spreading**
240 Previous work has clearly associated activation of ChvG-ChvI to a specific
241 transcriptomic pattern involving downregulation of flagellar motility genes and
242 upregulation of T6SS and succinoglycan biosynthesis genes [9,11,24]. Indeed, this
243 same pattern was observed in the 6- and 16-hour PBP1a depletion datasets (Fig 4A).
244 To confirm that the spreading phenotype is unrelated to flagella-dependent motility, we
245 made an in-frame deletion of *rem*, which encodes a transcriptional regulator of genes
246 encoding structural flagella proteins [25,26], in the PBP1a depletion strain. Deletion of
247 *rem* prevents swimming in *A. tumefaciens* and does not impact microcolony formation
248 on agarose pads (Fig 4B). Upon depletion of PBP1a, *rem* mutants continued to spread,
249 suggesting that the cause of this phenotype is independent of flagella-mediated
250 swimming motility (Fig 4B).

251 All genes in the *imp* and *hcp* operons, which are located on the linear
252 chromosome and encode the structural and toxin proteins of T6SS respectively, are
253 upregulated at both timepoints (Fig 4A). In *A. tumefaciens*, activation of the T6SS
254 results in the production of a contractile nanomachine which delivers effector proteins to
255 antagonize and compete with other bacteria [27]. Among agrobacteria, T6SS is
256 activated by different signals, is important during different stages of the lifecycle, and
257 may be used to acquire nutrients [28]. To determine if the T6SS contributes to the
258 spreading response observed during PBP1a depletion we deleted the intergenic gap
259 between the *hcp* and *imp* operons (ΔT6SSpro). This deletion prevented expression of
260 proteins from both the *hcp* and *imp* operons (Fig S5) [29]. Cell spreading persisted in
261 ΔT6SSpro during depletion of PBP1a suggesting that the activation of T6SS is not
262 responsible for this behavior.
263 Another possibility is that spreading might be caused by sliding motility, where
264 secretion of a surfactant gives the cells a slippery surface to “slide” across. Notably, *S.*
265 *meliloti* has been reported to undergo entropy-driven surface spreading during the
266 overproduction of succinoglycan [30]. Succinoglycan is a β-1,4-linked sugar made of
267 glucose and galactose, and is the most abundant exopolysaccharide produced by *A.*
268 *tumefaciens* and related bacteria [31]. Genes associated with the biosynthesis and
269 secretion of succinoglycan were strongly upregulated in both timepoints. To test if
270 entropy-driven surface spreading is causing PBP1a-depleted *A. tumefaciens* cells to
271 spread, we used a microscopy-based assay to observe succinoglycan production in *A.*
272 *tumefaciens*. Cells were spotted on agarose pads containing calcofluor white and grown
273 overnight, then imaged using the DAPI filter to detect succinoglycan production (Fig

274 4C). Wild-type *A. tumefaciens* and the PBP1a replete strains secrete some
275 succinoglycan that enriched near the center of the microcolony (Fig 4C). In comparison,
276 depletion of PBP1a triggers secretion of a large quantity of succinoglycan that defines
277 the boundary of where the cells spread. An in-frame deletion of *exoA*, which encodes a
278 glycosyltransferase required for succinoglycan production in *A. tumefaciens* [32],
279 prevents succinoglycan production (Fig 4D). During PBP1a depletion, microcolony
280 formation is restored in the Δ*exoA* mutant (Fig 4D). Together, these data illustrate that
281 succinoglycan is indeed overproduced and contributes to the surface spreading of the
282 PBP1a depletion.
283
284 **Deletion of *chvG* or *chvI* results in hypersensitivity to β-lactam antibiotics**
285 Since activation of succinoglycan production is known to be part of the ChvG-
286 ChvI regulon, we next wanted to test if the PBP1a depletion is activating SGN
287 production through the ChvG-ChvI signaling pathway. We made an in-frame deletion of
288 *chvI* in the PBP1a depletion background and found *chvI* mutants repleted with PBP1a
289 appear morphologically wild-type when grown in minimal media (Fig S6A). However,
290 PBP1a-depleted Δ*chvI* cells were extremely sick. Previously we reported that the
291 PBP1a depletion produces viable daughter cells for up to 5-6 generations [16], however,
292 the PBP1a-depleted Δ*chvI* strain was incapable of a single division event. Instead, the
293 cells exhibited growth arrest and eventually cell lysis shortly after depletion initiation (Fig
294 S6A, Movie S2).
295 To further assess the enhanced sensitivity of Δ*chvI* to PBP1a depletion, we
296 identified an antibiotic that specifically targets PBP1a enzymatic activity. Treatment with

297 cefsulodin at a concentration of 20 µg/mL resulted in a spreading phenotype similar to
298 the PBP1a depletion (Fig 5A). Additionally, treatment with cefsulodin results in short,
299 round cells, further phenocopying the PBP1a depletion (Fig 5B). Together, these data
300 suggest that cefsulodin targets the transpeptidase activity of PBP1a in *Agrobacterium*
301 *tumefaciens*, similar to reported cefsulodin specificity in *E. coli* [33]. Next, we observed
302 relative cefsulodin sensitivities in WT, Δ*chvG*, Δ*chvI*, and Δ*exoR* strains. Remarkably,
303 we found that while growth of wild-type and Δ*exoR* cells appeared relatively unaffected
304 by treatment with 10µg/mL of cefsulodin, Δ*chvG* and Δ*chvI* cells were hypersensitive
305 (Fig 4C). Next, we targeted the glycosyltransferase activity of PBP1a through treatment
306 with moenomycin [34], and found that moenomycin-treated cells also spread on
307 agarose pads (Fig S6B). These findings suggest that the ChvG-ChvI TCS is essential
308 for growth when the activity of the major PG synthase is inhibited either chemically or
309 genetically.
310 We broadened our investigation by testing Δ*chvG* and Δ*chvI* against ten
311 additional antibiotics. four that block protein synthesis (chloramphenicol, tetracycline,
312 erythromycin, and gentamicin); one that blocks DNA replication (nalidixic acid); one that
313 blocks transcription (rifampin); and four other cell wall synthesis inhibiting β-lactam
314 antibiotics (meropenem, cefoxitin, ampicillin, and ticarcillin). To measure changes in
315 sensitivity to each antibiotic compared to wildtype, Δ*chvG* and Δ*chvI* were spread on
316 ATGN minimal media and disks containing each antibiotic were applied. Diameters of
317 the zones of inhibition (ZOI) were measured and the difference in ZOIs for each mutant
318 strain compared to wildtype are shown (Fig 5D). Of the antibiotics tested, Δ*chvG* and

319 Δ*chvI* showed increased sensitivity only to β-lactam antibiotics, suggesting specificity of
320 the ChvG-ChvI pathway in conferring resistance to this antibiotic class.
321
322 **ChvG and ChvI are conserved in Alphaproteobacteria but the presence of ExoR is**
323 **more constrained**
324 The absence of PBP1a activity at the growth pole during elongation activates
325 ChvG-ChvI, the canonical host-invasion pathway of *Agrobacterium tumefaciens*. The
326 ChvG-ChvI pathway is most well known to be activated by environmental changes
327 associated with conditions favorable for plant association, yet this TCS is retained in
328 many non-plant-associated Alphaproteobacteria (Fig 6A). Remarkably, while ChvG-
329 ChvI is conserved in a large proportion of Alphaproteobacteria, ExoR is not (Fig 6A).
330 Predicted structures of the sensor domains of ChvG in bacteria with ChvG-ChvI
331 orthologs show two structural loops (L1 and L2; Fig 6A, Fig S7). While L2 is conserved
332 across the orthologous structures, L1 is expanded solely in the Rhizobiales (Fig S8).
333 This expansion coincides with the retention of ExoR, making it a compelling target for
334 ExoR-ChvG association studies (Fig 6A). The more broadly conserved L2, on the other
335 hand, may enable a conserved, ExoR-independent mechanism for activation of ChvG-
336 ChvI.
337 We hypothesized that the ChvG-ChvI pathway may confer resistance to cell wall
338 stress in other host-associated Rhizobiales. Indeed, depletion of PBP1a in
339 *Sinorhizobium meliloti* causes cells to spread suggest activation of ChvG-ChvI (ExoS-
340 ChvI) pathway (Fig 6B). Like *A. tumefaciens*, this response is specific to depletion of
341 PBP1a and is not triggered by deletion of the 5 other high molecular weight PBPs.

342 These results suggest that cell wall stress may be a well conserved trigger for activation
343 of ChvG-ChvI pathways in the Rhizobiales. Notably, *C. crescentus* does not spread
344 upon treatment with 80 μg/mL of cefsulodin (Fig S6C), despite recent findings that
345 ChvGI likely confers resistance at this concentration [12]. While *S. meliloti* and *A.*
346 *tumefaciens* encode succinoglycan biosynthesis operons, *C. crescentus* does not.
347 These findings support the hypothesis that the ChvG-ChvI response to cell wall stress is
348 conserved across Alphaproteobacterial species that have orthologs of ChvG-ChvI.
349

350 **DISCUSSION**

351 Why is ChvG-ChvI TCS activated upon inhibition of polar PG synthesis in *A.*
352 *tumefaciens*? PBP1a depletion results in a compositional shift in cell wall muropeptide
353 composition and cell wall crosslinking [16]. Here we find that PBP1a depletion causes
354 upregulation in transcription of LD-transpeptidases, endopeptidases, and soluble lytic
355 transglycosylases, indicating cells are attempting to compensate for compromised cells
356 walls. Remarkably, transcripts from these same genes are upregulated in the Δ*exoR*
357 and pH 5.5 datasets, suggesting that remodeling of the cell wall is a part of the ChvG-
358 ChvI regulon. While the role of cell wall remodeling during host-invasion is unclear it is
359 possible that these modifications may be protective for the bacterium when host
360 associated. The upregulation in transcription of genes encoding AopB and the Tol/Pal
361 system may indicate that PBP1a-depleted cells are succumbing to osmotic pressure, a
362 possible explanation for the increase in cell width in PBP1a-depleted and cefsulodin-
363 treated cells (Fig 5B). Notably, this concept aligns well with recent findings in
364 *Caulobacter crescentus* where it was shown that ChvGI activation was required for

365 osmoregulation [35]. Together, these findings indicate a conserved role within the
366 Alphaproteobacteria for the ChvG-ChvI TCS in sensing and responding to envelope
367 stress. Possible signals may include the accumulation of cytoplasmic peptidoglycan
368 precursors such as lipid II, increased levels of naked glycan strands in the cell wall, the
369 production of peptidoglycan hydrolysis products, or more conventional stress responses
370 due to osmotic sensitivity [36]. Future investigations will be necessary to determine if
371 ChvG-ChvI proteins themselves directly sense and respond to cell wall stress or if other
372 regulators which, presumably interact with the ChvG-ChvI are involved in this response.
373 If there is a conserved role in sensing cell wall stress, why would this pathway be
374 required for host invasion within *Agrobacterium tumefaciens*? One explanation could be
375 that during plant colonization, *A. tumefaciens* decreases cell wall biogenesis to form
376 cells which are relatively persistent in order to evade host recognition and survive the
377 harsh *in plantae* environment [37]. Alternatively, perhaps the integrity and composition
378 of the cell wall is routinely monitored and used as a signal for the activation of pathways
379 associated with lifestyle choice. Decreased activity of PBP1a may mimic one or more of
380 the conditions *A. tumefaciens* and *S. meliloti* encounter during host-invasion, leading to
381 the activation of ChvG-ChvI. Alternatively, perhaps the absence of PBP1a activity leads
382 to a destabilization of the polar growth complex leading to decreased cell envelope
383 integrity. It will be of interest to determine if other components of the polar growth
384 complex such as GPR [38], RgsP [39], or PopZ [40,41] have increased sensitivity to β-
385 lactam antibiotics and induce surface spreading. This possibility is in agreement with the
386 observation in *C. crescentus* that resistance to cell wall targeting antibiotics is
387 dependent on factors such as TipN that maintain the integrity of the cell envelope [42].

388 The overproduction of succinoglycan provides cells with passive protection
389 against several stresses *A. tumefaciens* may encounter during host invasion including
390 detergents, salt, acidity, heat, antimicrobial peptides, and reactive oxygen species [33-
391 36]. Production of succinoglycan may also help protect against cell-wall-synthesis
392 targeting antibiotics produced by competing bacteria and fungi in the soil. However,
393 succinoglycan production is taxonomically constrained within plant-host-associated
394 bacteria, indicating that there are other conserved mechanisms regulated by ChvG-ChvI
395 in resistance to these antibiotics. The surface spreading phenomenon that we
396 connected to overproduction of succinoglycan and that has been previously described
397 in *S. meliloti* [30], may be involved in cell dispersal during host invasion.
398 The increased sensitivity to mecillinam, vancomycin, cefsulodin, and
399 moenomycin in ChvGI mutants suggests that this pathway may confer resistance to
400 antibiotics inhibiting cell wall synthesis [35]. Our observation that the depletion of *A.*
401 *tumefaciens* RgsM mutant does not induce surface spreading further hints that
402 increased cell wall hydrolysis may be responsible for activation of the ChvG-ChvI
403 pathway. While our findings suggest a conserved signal in ChvG-ChvI activation, further
404 studies will need to be conducted to identify the signal(s), determine if they are species-
405 specific, and explore the conditions which lead to signal production.
406 Longer depletions of PBP1a may induce a more general stress response. While
407 previous reports propose *A. tumefaciens* to have stress-specific responses instead of a
408 single general response [43] , the similarities between the transcriptional changes at the
409 16-hour time point and the general stress responses of other bacteria are striking [44].
410 For example, the general stress response of *Escherichia coli*, regulated by the ECF

411 family sigma factor σ^E, upregulates transcription of genes encoding ABC transporters
412 associated with uptake of amino acids, peptides, phosphate sources, and polyamines
413 [45]. Indeed, the 16-hour time point shows differential expression of over 30 ABC
414 transporters. However, previous studies found no common response to stresses
415 including osmotic stress, heat shock, and low pH in *A. tumefaciens* [43]. While there are
416 several ECF family sigma factors encoded in the *A. tumefaciens* genome, it is unclear
417 what, if any, role they may be playing in the transcriptional changes exhibited under
418 long depletions of PBP1a.

419 Together our findings support a model that ChvG-ChvI can be acid induced by
420 dissociation and proteolysis of ExoR in a Rhizobiales specific response (Fig 6C, left)
421 and through a more broadly conserved cell envelope stress response (Fig 6C, middle).
422 The role of ExoR regulation is well established for the acid-induction of ChvG-ChvI but
423 the lack of ExoR conservation suggests that the cell envelope stress response may be
424 ExoR-independent. Finally, longer periods of PBP1a depletion results in a more general
425 stress response, affecting transcription of genes associated with nutrient uptake and
426 metabolism (Fig 6C, right). Overall, the data presented here are in agreement with
427 recent works in *Caulobacter* [35,42] which suggest that ChvGI activation is important in
428 oligotrophic free-living bacteria as a cell envelope or osmotic stress response.
429 Remarkably, it seems that the ChvG-ChvI pathway has a dual purpose in protecting the
430 bacterium and invading its host in *A. tumefaciens*, and other host-associated
431 Rhizobiales.

432

433 **MATERIALS AND METHODS**

434 **Bacterial strains, plasmids, and growth conditions.** A list of all bacterial strains and
435 plasmids used in this study is provided in Table S2. *Agrobacterium tumefaciens* C58
436 and derived strains were grown in ATGN minimal media [46] without exogenous iron at
437 28°C with shaking. When appropriate, kanamycin (KAN) was used at the working
438 concentration of 300 µg/ml. When indicated, isopropyl β-D-1-thio-galactopyranoside
439 (IPTG) was used as an inducer at a concentration of 1 mM, and cumate. *Sinorhizobium*
440 *meliloti* stains were grown in TY medium [47] at 28°C. When appropriate, KAN was
441 used at the working concentration of 200 µg/ml, gentamycin (GM) was used at 20
442 µg/ml, and IPTG was used at a concentration of 500 µg/ml. *C. crescentus* strains were
443 grown in PYE medium [48] at 28°C. *E. coli* DH5α and S17-1 λ pir were grown in Luria-
444 Bertani medium at 37°C and when appropriate 50 µg/ml or 30 µg/ml of KM were added,
445 respectively.
446
447 **Construction of deletion/depletion plasmids and strains.** A list of all primers and
448 synthetic DNAs used in this study is provided in Table S3. Vectors for gene deletion by
449 allelic exchange were constructed using recommended methods for *A. tumefaciens*
450 [49]. Briefly, 500-bp fragments upstream and 500 bp downstream of the target gene
451 were amplified using primer pairs P1/P2 and P3/4 respectively. Amplicons were spliced
452 together by SOEing using primer pair P1/P4. The amplicon was digested and ligated
453 into pNTPS139. The deletion plasmids were introduced into *A. tumefaciens* by mating
454 using an *E. coli* S17 conjugation strain to create KM resistant, sucrose sensitive primary
455 integrants. Primary integrants were grown overnight in media with no selection.
456 Secondary recombinants were screened by patching for sucrose resistance and KM

457 sensitivity. Colony PCR with primers P5/P6 for the respective gene target was used to
458 confirm deletion. PCR products from P5/P6 primer sets were sequenced to further
459 confirm deletions.
460
461 **Phase and fluorescence microscopy.** A small volume (~1 µl) of cells in exponential
462 phase (OD600 = 0.2 - 0.4) was applied to a 1% ATGN agarose pad as described
463 previously [50]. DIC, Phase contrast and epifluorescence microscopy were performed
464 with an inverted Nikon Eclipse TiE and a QImaging Rolera em-c2 123 1K EMCCD
465 camera with Nikon Elements Imaging Software. For time-lapse microscopy, images
466 were collected every ten minutes, unless otherwise stated. For calcofluor agar pad
467 assays, calcofluor was added to agarose pads at a concentration of 25 µg/mL and
468 exposed to DAPI filter for 50ms. When appropriate agar pads were supplemented with
469 1mM IPTG. For quantitative image analysis, live cells were imaged using phase-
470 contrast microscopy, and cell length and width distributions of the indicated number of
471 cells per strain were determined as measured using MicrobeJ software [51]. T-tests
472 were performed using the compare_means() function of the ggpubr R library.
473
474 **RNA isolation, sequencing and analysis.** Four cultures each of WT, WT + IPTG and
475 12 cultures of + PBP1a depletion cells were grown overnight in 2 ml of ATGN minimal
476 media at 28°C with shaking; the + PBP1a strains and WT + IPTG strains were
477 supplemented with 1mM IPTG. Cells were then pelleted by centrifugation at 7000 x g for
478 5 minutes. Cell pellets were washed three times with ATGN by centrifugation and
479 resuspension to remove IPTG. After the final wash the cell pellets from WT, WT + IPTG,

480 and four of the 12 + PBP1a strains were resuspended to an OD600 of 0.05 in 6mL
481 ATGN, or ATGN with 1mM IPTG. The other eight + PBP1a strains were resuspended to
482 an OD600 of 0.05 in 6 ml ATGN without IPTG. This resulted in 4 replicate cultures each
483 of WT, WT +IPTG, + PBP1a, - PBP1a_6hr and - PBP1a_16hr. Growth of the cultures
484 was monitored and supplemented with fresh medium as needed so that the OD600
485 never went over 0.3. RNA was isolated from the -PBP1a_6hr strains after 6 hours of
486 growth, and RNA was isolated from all other strains after 16 hours of growth. To
487 prepare samples, a culture volume equivalent to 6 ml at an optical density at 600 nm
488 (OD600) of 0.2-0.3 was pelleted by centrifugation at 7000 x g for 5 minutes and pellets
489 were resuspended in 1mL of ATGN media and incubated with 2 mL of RNAProtect
490 reagent (QIAgen) for 15 min at room temperature. Cells were lysed with 10 mg
491 lysozyme, and RNA was extracted using the QIAgen RNEasy kit.
492
493 DNA libraries for sequencing were constructed following the manufacturer's protocol
494 with reagents supplied in Illumina's TruSeq mRNA stranded sample preparation kit. The
495 sample concentration was determined by Qubit flourometer (Invitrogen) using the Qubit
496 HS RNA assay kit, and the RNA integrity was checked using the Fragment Analyzer
497 automated electrophoresis system. Briefly, the poly-A containing mRNA is purified from
498 total RNA, RNA is fragmented, double-stranded cDNA is generated from fragmented
499 RNA, and the index containing adapters are ligated to the ends. The amplified cDNA
500 constructs were purified by addition of Axyprep Mag PCR Clean-up beads. The final
501 construct of each purified library was evaluated using the Fragment Analyzer automated
502 electrophoresis system, quantified with the Qubit flourometer using the Qubit HS dsDNA

503 assay kit, and diluted according to Illumina's standard sequencing protocol for
504 sequencing on the NextSeq 500.
505
506 For all samples, when adapter sequence was detected, it was removed using cutadapt
507 (0.16) [52]. All samples were purged of reads that mapped to transcripts for rRNA genes
508 using bowtie2 (2.3.4.3) [53]. The reads were then mapped to the *A. fabrum* str. C58
509 genome using STAR (version 2.5.4b) [54], which also produces the number of read
510 counts per gene. The index files used by STAR were derived from the files
511 *Agrobacterium*_fabrum_str_c58.ASM9202v1.dna.toplevel.fa and
512 *Agrobacterium*_fabrum_str_c58.ASM9202v1.40.gtf, both of which are part of Ensembl
513 release 40 (http://bacteria.ensembl.org/index.html). Pairwise comparisons were
514 performed to test for differential expression of genes using the Bioconductor package
515 DESeq2 [55]. Gene annotations were collected from the annotations included with the
516 file of cDNAs also at Ensembl
517 *Agrobacterium*_fabrum_str_c58.ASM9202v1.cdna.all.fa.gz.
518
519 **COG functional annotation.** Amino acid sequences for all proteins in *A. tumefaciens*
520 were downloaded in a single FASTA file from GenBank and uploaded to EGGNOG-
521 MAPPER [56,57]. COG terms were outputted, and Python code was written to pull out
522 transcripts from 16-hour depletion of PBP1a with L2FC > 2.0 or < -2.0. Some transcripts
523 had multiple COG annotations and were therefore replicated for visualization according
524 to the number of annotations it had.
525

526 **Comparative transcriptomics.** Transcripts and L2FC values from each dataset were
527 opened in Python code written to screen for and exclude any genes that were not
528 present in both datasets. Statistics and visualization was done in R. Spearman
529 correlation statistical test was run on the L2FC of the 150 most differentially expressed
530 genes in the PBP1a depletion and their corresponding L2FC values in the comparison
531 dataset.
532
533 **Cell viability assays.** For cell viability spot assays, cultures were grown overnight and
534 diluted to an OD_{600} = 0.05 and serially diluted in ATGN and spotted on ATGN agar
535 plates containing antibiotics as indicated. Four microliters of each dilution was spotted
536 and plates were incubated at 28°C for 48 h before imaging.
537
538 **Disk diffusion assays.** Wild-type, Δ*chvG*, and Δ*chvI* cells were overnight and then
539 knocked down to an OD_{600} of 1.0. Cells were then lawned on ATGN minimal media.
540 Sterile paper disks either soaked in concentrations of each antibiotic or not (blank
541 controls) were applied to the plate. Each plate was grown for ~48 hours at 28°C before
542 being imaged. Zone of inhibition diameters were measured from each image using
543 ImageJ software.
544
545 **Phylogenetics and structure prediction.** A seed of 22 amino acid sequences
546 containing the annotated ChvG sensor domain (PF13755) were initially downloaded
547 from Pfam [58]. Each was blasted against its corresponding proteome to retrieve the full
548 protein sequence [59]. Additional sequences of relevant bacteria such as *S. meliloti,*

549 *Brucella melitensis,* and *C. crescentus,* were added by blasting the amino acid
550 sequence from *A. tumefaciens* ChvG (Atu0033) against each organism's proteome. All
551 sequences were aligned using MUSCLE and trimmed in Jalview according to Uniprot
552 predicted periplasmic region of Atu0033 [60–62]. A maximum parsimony phylogenetic
553 tree of these sequences was generated using MEGA-X [63].
554
555 Each trimmed sequence underwent one-to-one threading in Phyre2 with the complete
556 structure of Atu0033 predicted by AlphaFold as a template [64,65]. Local alignment and
557 a secondary structure weight of 0.1 was used. Structural analysis and structure
558 alignment was done in ChimeraX [66].
559
560 The amino acid sequence of *A. tumefaciens* ExoR (Atu1715) was blasted against each
561 organism's proteome and max score values of top hits were recorded. Max score values
562 under 50 were deemed too different and were therefore not considered an ExoR
563 ortholog. Additionally, sequences of each top hit were blasted against the proteome of
564 *A. tumefaciens.* If the top hit was not ExoR, it was also not considered an ExoR ortholog
565 in this analysis.
566
567 **DATA AVAILABILITY**
568 Raw RNA-seq read files (.fastq) and complete list of differentially expressed genes for each
569 comparison are publicly available through the NCBI Gene Expression Omnibus (GEO) under
570 the accession GSE173921.
571
572 **ACKNOWLEDGEMENTS**

We thank Elizaveta Krol and Anke Becker for providing *Sinorhizobium meliloti* strains and micrographs and Erh-Min Lai for providing antibodies used in this work. We thank Amelia Randich, Alex Quintero, Regis Hallez and members of the Brown lab for critical feedback on this manuscript. This work was supported by the National Science Foundation, IOS1557806, to PJBB. MAW and JMB were supported by the Life Sciences Fellowship at the University of Missouri and AKM was supported as an IMSD/MARC fellow with support from the National Institutes of Health, T34 GM136493.

The molecular graphics and analyses were performed with UCSF ChimeraX, developed by the Resource for Biocomputing, Visualization, and Informatics at the University of California, San Francisco, with support from National Institutes of Health R01-GM129325 and the Office of Cyber Infrastructure and Computational Biology, National Institute of Allergy and Infectious Diseases.

REFERENCES

1. Venturi V, Keel C. Signaling in the Rhizobiales. Trends Plant Sci. 2016;21: 187–198.
2. Capra EJ, Laub MT. Evolution of two-component signal transduction systems. Annu Rev Microbiol. 2012;66: 325–347.
3. Yuan Z-C, Haudecoeur E, Faure D, Kerr KF, Nester EW. Comparative transcriptome analysis of *Agrobacterium tumefaciens* in response to plant signal salicylic acid, indole-3-acetic acid and γ-amino butyric acid reveals signalling cross-talk and *Agrobacterium*-plant co-evolution. Cell Microbiol. 2008;10: 2339–2354.
4. Cho H, Winans SC. VirA and VirG activate the Ti plasmid *repABC* operon, elevating plasmid copy number in response to wound-released chemical signals. Proc Natl Acad Sci U S A. 2005;102: 14843–14848.
5. Xue S, Biondi EG. Coordination of symbiosis and cell cycle functions in *Sinorhizobium meliloti*. Biochim Biophys acta Gene Regul Mech. 2019;1862: 691–696.
6. Heavner ME, Qiu W-G, Cheng H-P. Phylogenetic co-occurrence of ExoR, ExoS, and ChvI, components of the RSI bacterial invasion switch, suggests a key

605 adaptive mechanism regulating the transition between free-living and host-
606 invading phases in Rhizobiales. Mergaert P, editor. PLoS One. 2015;10:
607 e0135655.
608 7. Wells DH, Chen EJ, Fisher RF, Long SR. ExoR is genetically coupled to the
609 ExoS-ChvI two-component system and located in the periplasm of *Sinorhizobium*
610 *meliloti*. Mol Microbiol. 2007;64: 647–664.
611 8. Lu HY, Luo L, Yang MH, Chenga HP. *Sinorhizobium meliloti* ExoR is the target of
612 periplasmic proteolysis. J Bacteriol. 2012;194: 4029–4040.
613 9. Yuan ZC, Liu P, Saenkham P, Kerr K, Nester EW. Transcriptome profiling and
614 functional analysis of *Agrobacterium tumefaciens* reveals a general conserved
615 response to acidic conditions (pH 5.5) and a complex acid-mediated signaling
616 involved in *Agrobacterium*-plant interactions. J Bacteriol. 2008;190: 494–507.
617 10. Alakavuklar MA, Heckel BC, Stoner AM, Stembel JA, Fuqua C. Motility control
618 through an anti-activation mechanism in *Agrobacterium tumefaciens*. Mol
619 Microbiol. 2021;116: 1281–1297.
620 11. Heckel BC, Tomlinson AD, Morton ER, Choi JH, Fuqua C. *Agrobacterium*
621 *tumefaciens* ExoR controls acid response genes and impacts exopolysaccharide
622 synthesis, horizontal gene transfer, and virulence gene expression. J Bacteriol.
623 2014;196: 3221–3233.
624 12. Quintero-Yanes A, Mayard A, Hallez R. The two-component system ChvGI
625 maintains cell envelope homeostasis in *Caulobacter crescentus*. bioRxiv. 2022;
626 2022.01.18.476748.
627 13. Vallet SU, Hansen LH, Bistrup FC, Laursen SA, Chapalay JB, Chambon M, et al.
628 Loss of bacterial cell pole stabilization in *Caulobacter crescentus* sensitizes to
629 outer membrane stress and peptidoglycan-directed antibiotics. MBio. 2020;11.
630 14. Brown PJB, De Pedro MA, Kysela DT, Van Der Henst C, Kim J, De Bolle X, et al.
631 Polar growth in the Alphaproteobacterial order Rhizobiales. PNAS. 2012;109:
632 1697-1701.
633 15. Margolin W. Sculpting the Bacterial Cell. Curr Biol. 2009;19: R812.
634 16. Williams MA, Aliashkevich A, Krol E, Kuru E, Bouchier JM, Rittichier J, et al.
635 Unipolar Peptidoglycan Synthesis in the Rhizobiales Requires an Essential Class
636 A Penicillin-Binding Protein. 2021;12.
637 17. Figueroa-Cuilan WM, Randich AM, Dunn CM, Santiago-Collazo G, Yowell A,
638 Brown PJB. Diversification of LytM in and of *Agrobacterium tumefaciens*. Front
639 Microbiol. 2021;12: 2341.
640 18. Krol E, Yau HCL, Lechner M, Schäper S, Bange G, Vollmer W, et al. Tol-pal
641 system and proteins interact to promote unipolar growth and cell division in
642 *Sinorhizobium meliloti*. MBio. 2020;11: 1–21.
643 19. Tatusov RL, Koonin E V., Lipman DJ. A genomic perspective on protein families.
644 Science. 1997;278: 631–637.
645 20. Galperin MY, Kristensen DM, Makarova KS, Wolf YI, Koonin E V. Microbial
646 genome analysis: the COG approach. Brief Bioinform. 2019;20: 1063.
647 21. Chaoprasid P, Dokpikul T, Johnrod J, Sirirakphaisarn S, Nookabkaew S,
648 Sukchawalit R, et al. *Agrobacterium tumefaciens* Zur regulates the high-affinity
649 zinc uptake system TroCBA and the putative metal chaperone YciC, along with
650 ZinT and ZnuABC, for survival under zinc-limiting conditions. Appl Environ

651 Microbiol. 2016;82: 3503.
652 22. Yuan Z-C, Edlind MP, Liu P, Saenkham P, Banta LM, Wise AA, et al. The plant
653 signal salicylic acid shuts down expression of the *vir* regulon and activates
654 quormone-quenching genes in *Agrobacterium*. 2007;104: 11790-11795
655 23. Haryono M, Cho ST, Fang MJ, Chen AP, Chou SJ, Lai EM, et al. Differentiations
656 in gene content and expression response to virulence induction between two
657 Front Microbiol. 2019;10: 1554.
658 24. Wu CF, Lin JS, Shaw GC, Lai EM. Acid-induced Type VI Secretion System is
659 regulated by ExoR-ChvG. PLoS Pathog. 2012;8.
660 25. Figueroa-Cuilan W, Daniel JJ, Howell M, Sulaiman A, Brown PJB. Mini-Tn7
661 insertion in an artificial attTn7 site enables depletion of the essential master
662 regulator CtrA in the phytopathogen *Agrobacterium tumefaciens*. Appl Environ
663 Microbiol. 2016;82: 5015–5025.
664 26. Rotter C, Mühlbacher S, Salamon D, Schmitt R, Scharf B. Rem, a new
665 transcriptional activator of motility and chemotaxis in *Sinorhizobium meliloti*. J
666 Bacteriol. 2006;188: 6932.
667 27. Wu CF, Smith DA, Lai EM, Chang JH. The *Agrobacterium* Type VI Secretion
668 System: a contractile nanomachine for interbacterial competition. 2018;418: 215–
669 231.
670 28. Wu CF, Weisberg AJ, Davis EW, Chou L, Khan S, Lai EM, et al. Diversification of
671 the Type VI Secretion System in Agrobacteria. MBio. 2021;12.
672 29. Lin JS, Ma LS, Lai EM. Systematic Dissection of the *Agrobacterium* Type VI
673 Secretion System reveals machinery and secreted components for subcomplex
674 formation. PLoS One. 2013;8: e67647.
675 30. Dilanji GE, Teplitski M, Hagen SJ. Entropy-driven motility of *Sinorhizobium meliloti*
676 on a semi-solid surface. Proc R Soc B Biol Sci. 2014;281.
677 31. Mendis HC, Madzima TF, Queiroux C, Jones KM. Function of succinoglycan
678 polysaccharide in *Sinorhizobium meliloti* host plant invasion depends on
679 succinylation, not molecular weight. MBio. 2016;7.
680 32. Schmid J, Sieber V, Rehm B. Bacterial exopolysaccharides: Biosynthesis
681 pathways and engineering strategies. Front Microbiol. 2015;6: 496.
682 33. Curtis NAC, Orr D, Ross GW, Boulton MG. Affinities of penicillins and
683 cephalosporins for the penicillin-binding proteins of *Escherichia coli* K-12 and their
684 antibacterial activity. Antimicrob Agents Chemother. 1979;16: 533.
685 34. Yuan Y, Fuse S, Ostash B, Sliz P, Kahne D, Walker S. Structural analysis of the
686 contacts anchoring moenomycin to peptidoglycan glycosyltransferases and
687 implications for antibiotic design. 2008;3: 429–436.
688 35. Quintero-Yanes A, Coppine J, Mayard A, Hallez R. The two-component system
689 ChvGI maintains cell envelope homeostasis in *Caulobacter crescentus*. bioRxiv.
690 2022.
691 36. Piepenbreier H, Diehl A, Fritz G. Minimal exposure of lipid II cycle intermediates
692 triggers cell wall antibiotic resistance. Nat Commun 2019 101. 2019;10: 1–13.
693 37. Erbs G, Silipo A, Aslam S, De Castro C, Liparoti V, Flagiello A, et al.
694 Peptidoglycan and muropeptides from pathogens *Agrobacterium* and
695 Xanthomonas elicit plant innate immunity: Structure and Activity. Chem Biol.
696 2008;15: 438–448.

38. Zupan JR, Grangeon R, Robalino-Espinosa JS, Garnica N, Zambryski P. GROWTH POLE RING protein forms a 200-nm-diameter ring structure essential for polar growth and rod shape in *Agrobacterium tumefaciens*. Proc Natl Acad Sci U S A. 2019;166: 10962–10967.
39. Schäper S, Yau HCL, Krol E, Skotnicka D, Heimerl T, Gray J, et al. Seven-transmembrane receptor protein RgsP and cell wall-binding protein RgsM promote unipolar growth in Rhizobiales. PLOS Genet. 2018;14: e1007594.
40. Howell M, Aliashkevich A, Salisbury AK, Cava F, Bowman GR, Brown PJB. Absence of the Polar Organizing Protein PopZ Results in Reduced and Asymmetric Cell Division in *Agrobacterium tumefaciens.* Journal of Bacteriology. 2017;199.
41. Grangeon R, Zupan J, Jeon Y, Zambryski PC. Loss of PopZAt activity in *Agrobacterium tumefaciens* by deletion or depletion leads to multiple growth poles, minicells, and growth defects. MBio. 2017;8.
42. Vallet SU, Hansen LH, Bistrup FC, Laursen SA, Chapalay JB, Chambon M, et al. Loss of bacterial cell pole stabilization in *Caulobacter crescentus* sensitizes to outer membrane stress and peptidoglycan-directed antibiotics. MBio. 2020;11.
43. Rosen R, BÃ¼ttner K, Schmid R, Hecker M, Ron EZ. Stress-induced proteins of *Agrobacterium tumefaciens*. FEMS Microbiol Ecol. 2001;35: 277–285.
44. Hecker M, Völker U. General stress response of Bacillus subtilis and other bacteria. Adv Microb Physiol. 2001;44: 35–91.
45. Hayden JD, Ades SE. The extracytoplasmic stress factor, σE, is required to maintain cell envelope integrity in *Escherichia coli*. PLoS One. 2008;3: e1573.
46. Morton ER, Fuqua C. UNIT 3D.1 Laboratory Maintenance of *Agrobacterium*. Curr Protoc Microbiol. 2012.
47. Beringer JE. R factor transfer in *Rhizobium leguminosarum*. J Gen Microbiol. 1974;84: 188–198.
48. Poindexter P, J. BIOLOGICAL PROPERTIES AND CLASSIFICATION OF THE CAULOBACTER GROUP. Bacteriol Rev. 1964;28: 231.
49. Morton ER, Fuqua C. Genetic manipulation of *Agrobacterium*. Curr Protoc Microbiol. 2012;Chapter 3.
50. Howell M, Daniel JJ, Brown PJB. Live cell fluorescence microscopy to bbserve essential processes during microbial cell growth. J Vis Exp. 2017;2017: 56497.
51. Ducret A, Quardokus EM, Brun Y V. MicrobeJ, a tool for high throughput bacterial cell detection and quantitative analysis. Nat Microbiol. 2016;1.
52. Martin M. Cutadapt removes adapter sequences from high-throughput sequencing reads. EMBnet.journal. 2011;17: 10–12.
53. Langmead B, Salzberg SL. Fast gapped-read alignment with Bowtie 2. Nat Methods. 2012;9: 357–359.
54. Dobin A, Gingeras TR. Mapping RNA-seq reads with STAR. Curr Protoc Bioinforma. 2015;51: 11.14.1-11.14.19.
55. Love MI, Huber W, Anders S. Moderated estimation of fold change and dispersion for RNA-seq data with DESeq2. Genome Biol. 2014;15: 1–21.
56. Sayers EW, Bolton EE, Brister JR, Canese K, Chan J, Comeau DC, et al. Database resources of the national center for biotechnology information. Nucleic Acids Res. 2022;50: D20–D26.

57. Huerta-Cepas J, Szklarczyk D, Heller D, Hernández-Plaza A, Forslund SK, Cook H, et al. eggNOG 5.0: a hierarchical, functionally and phylogenetically annotated orthology resource based on 5090 organisms and 2502 viruses. Nucleic Acids Res. 2019;47: D309.
58. Mistry J, Chuguransky S, Williams L, Qureshi M, Salazar GA, Sonnhammer ELL, et al. Pfam: The protein families database in 2021. Nucleic Acids Res. 2021;49: D412–D419.
59. Johnson M, Zaretskaya I, Raytselis Y, Merezhuk Y, Mcginnis S, Madden TL. NCBI BLAST: a better web interface. Nucleic Acids Res. 2008;36: 5–9.
60. Edgar RC. MUSCLE: multiple sequence alignment with high accuracy and high throughput. Nucleic Acids Res. 2004;32: 1792.
61. Waterhouse AM, Procter JB, Martin DMA, Clamp M, Barton GJ. Jalview Version 2—a multiple sequence alignment editor and analysis workbench. Bioinformatics. 2009;25: 1189–1191.
62. Bateman A, Martin MJ, Orchard S, Magrane M, Agivetova R, Ahmad S, et al. UniProt: the universal protein knowledgebase in 2021. Nucleic Acids Res. 2021;49: D480–D489.
63. Kumar S, Stecher G, Li M, Knyaz C, Tamura K. MEGA X: Molecular evolutionary genetics analysis across computing platforms. Mol Biol Evol. 2018;35: 1547–1549.
64. Kelley LA, Mezulis S, Yates CM, Wass MN, Sternberg MJE. The Phyre2 web portal for protein modeling, prediction and analysis. Nat Protoc. 2015;10: 845–858.
65. Jumper J, Evans R, Pritzel A, Green T, Figurnov M, Ronneberger O, et al. Highly accurate protein structure prediction with AlphaFold. Nat 2021 5967873. 2021;596: 583–589.
66. Pettersen EF, Goddard TD, Huang CC, Meng EC, Couch GS, Croll TI, et al. UCSF ChimeraX: Structure visualization for researchers, educators, and developers. Protein Sci. 2021;30: 70–82.

SUPPORTING INFORMATION

Movie S1. Growth and morphological changes during 8 hours of PBP1a depletion. Cells were washed to remove inducer and spotted immediately on an ATGN pad. Images were acquired every ten minutes and movie is played at 16 frames per second for a total of 48 frames.

Movie S2. Growth and division of D*chvI* during PBP1a depletion. Cells were washed to remove inducer and spotted immediately on an ATGN pad. Images were acquired every five minutes and movie is played at 40 frames per second for a total of 200 frames.

Fig S1. Pelleting of PBP1a-depleted and repleted cells. Conical tubes show turbidity after pelleting cells grown for 16 hours in PBP1a replete (+PBP1a) or depleted (-PBP1a) conditions. Cells were centrifuged at 1690 x g (3000 rpm in TX-400 rotor in a Sorvall Legend X1R centrifuge) for 10 minutes. Supernatants were spotted on a 1.25% ATGN agarose pad. $\bar{x}$ = average number of cells from 10 fields of view.

789
790 **Fig S2. Analysis of the control transcriptomes by RNA-seq.** A. Plots comparing
791 Log2Fold Change of the WT 6-hour transcriptome to that of the WT +ITPG 6-hour
792 transcriptome. Gray dots represent a single transcript, and the dotted lines represent +/-
793 2.0 Log2Fold Change threshold. Plots are delimited by chromosomes and mega
794 plasmids. B. Plots comparing Log2Fold Change of the WT +IPTG transcriptome to that
795 of the PBP1a depletion strain with ITPG present to drive PBP1a expression.
796 Comparisons shown are of the 6-hour transcriptomes. Gray dots represent a single
797 transcript, and the dotted lines represent +/- 2.0 Log2Fold Change threshold. Plots are
798 delimited by chromosomes and mega plasmids.
799
800 **Fig S3. Transcriptional changes of TCS regulators and kinases during PBP1a**
801 **depletion.** The fold change in expression level of TCS regulators and kinases are
802 shown following 6 hours (gray) and 16 hours (black) of PBP1a depletion. The *virAG* and
803 *chvGI* TCS pairs are labeled.
804
805 **Fig S4. The response to the depletion of PBP1a mimics transcriptional changes**
806 **associated with host invasion.** A. Correlation scatterplots depicting relationships
807 between the log2fold-change (L2FC) values in the 16-hour PBP1a depletion and
808 transcriptomic data sets taken under simulated virulence-inducing conditions (AS) and
809 under simulated host-invading conditions (Δ*exoR*). Each point represents a unique
810 transcript. AS, acetosyrinogone; Rho, Spearman correlation coefficient. B. Correlation
811 scatterplots comparing L2FC values of transcripts in the pH 5.5 microarray, a condition
812 known to induce the *chvG-chvI* regulon, to either the 6-hour (red) or 16-hour (blue)
813 PBP1a depletion. Rho, Spearman correlation coefficient.
814
815 **Fig S5. Western blot of proteins expressed from the two type VI secretion system**
816 **operons in ΔT6SSpro strains.** Top panel, diagram of the two operons encoding
817 elements of Type VI Secretion in *A. tumefaciens.* T6SSpro labels the intergenic gap that
818 is deleted in ΔT6SSpro strains. Middle panel, western blots using anti-Hcp and anti-
819 TssB in each of the indicated strains. Protein sizes (kDa) are shown on the right. Bottom
820 panel, Coomassie stained gel showing total protein from each strain.
821
822 **Fig S6. Impact of decreased PG synthesis on *A. tumefaciens* and *C. crescentus***
823 **microcolony formation.** A. Micrographs of PBP1a depletion ∆*chvI* with (+PBP1A) or
824 without (-PBP1A) IPTG. Cells was grown to exponential phase in ATGN media
825 containing IPTG, spotted on an ATGN agar pad with or without IPTG, allowed to grow
826 for 16 hours, and imaged by DIC microscopy. B. Micrographs of WT *A. tumefaciens*
827 cells growth with or without moenomycin. Cells was grown to exponential phase in
828 ATGN media, spotted on an ATGN agar pad with or without moenomycin, allowed to
829 grow for 16 hours, and imaged by DIC microscopy. C. Micrographs of WT *C. crescentus*
830 cells growth with or without cefsulodin. Cells were grown to exponential phase in PYE
831 media, spotted on a PYE agar pad with or without cefsulodin, allowed to grow for 16
832 hours, and imaged by DIC microscopy. All scale bars depict 2μm.
833

834 **Fig S7. Alignment of periplasmic regions of ChvG orthologs.** Partial MUSCLE
835 alignment of ChvG ortholog periplasmic domains. Highlighted columns represent strong
836 conservation across aligned sequences. Atu0033 (ChvG of *A. tumefaciens)* is the
837 reference sequence for this analysis. L1 and L2 correspond to two conserved structural
838 loops. Conservation, quality, and consensus scores for each site are represented as bar
839 graphs under the alignment. Shading indicates order of the bacterium containing the
840 ChvG ortholog: Orange, Rhizobiales; Purple, Rhodobacterales; Green,
841 Caulobacterales; Gold, Rhodospirales.
842
843 **Fig S8. Structure predictions for the periplasmic regions of ChvG orthologs.**
844 Phyre2 structural predictions for each organism displayed in Figure 6A of this work.
845 Genus and species names as well as locus tags for each ChvG ortholog are provided.
846 Range of numbers following the back slash are the amino acid sites used in structure
847 prediction. Colors indicates order of the bacterium containing the ChvG ortholog:
848 Orange, Rhizobiales; Purple, Rhodobacterales; Green, Caulobacterales; Gold,
849 Rhodospirales.
850
851 **Table S1. Selected differentially expressed genes**
852
853 **Table S2. Bacterial strains and plasmids.**
854
855 **Table S3. Synthesized DNA primers.**
856
857 **Supplementary Methods**
858
859 **Supplementary References**

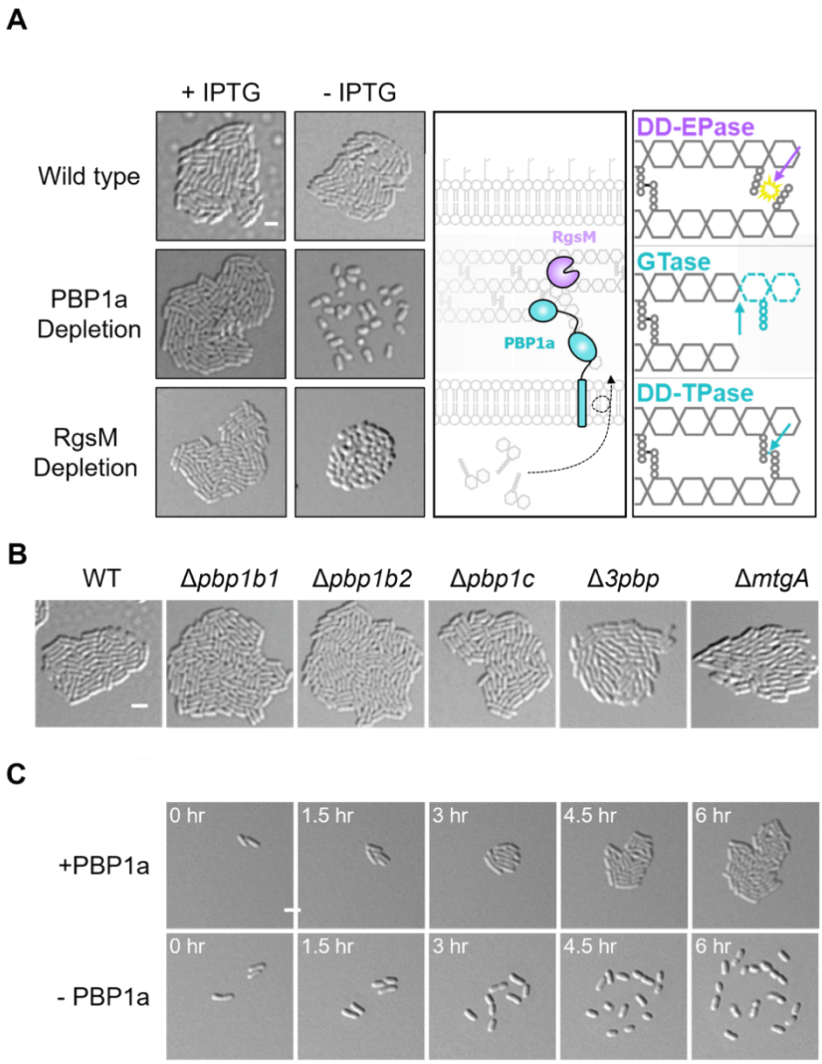

Fig 1. The PBP1a depletion fails to form microcolonies independent of flagellar motility. A. Micrographs of wildtype, PBP1a depletion, and RgsM depletion with or without 1mM IPTG inducer. Each strain was grown to exponential phase, spotted on an ATGN agar pad, allowed to grow for 16 hours, and imaged by DIC microscopy. Scale bar depicts 2μm. The graphic depicts the working model that RgsM $_{DD}$-endopeptidase activity is required for incorporation of nascent glycan strands into the preexisting peptidoglycan (PG) macromolecule by PBP1a. i) RgsM cleaves $_{DD}$-crosslinks, ii) PBP1a glycosyltransferase activity incorporates lipid II into the PG glycan strand, iii) PBP1a $_{DD}$-transpeptidase activity crosslinks the peptide stem of the nascent PG, fully incorporating it into the macromolecule. B. Micrographs of wild type, Δ*pbp1b1*, Δ*pbp1b2*, Δ*pbp1c*, and Δ*mtgA*. Each strain was grown to exponential phase, spotted on an ATGN agar pad, allowed to grow for 16 hours, and imaged by DIC microscopy. Scale bar depicts 2μm. C. Time-lapse microscopy of the PBP1a depletion grown on an agar pad with or without 1mM IPTG inducer. DIC images were acquired every 10 minutes. Time is shown in hours. For the - PBP1a strain, cells were washed 3X with ATGN media and grown at 28 C with shaking for 4 hours before cells were spotted on an agar pad for imaging.

878

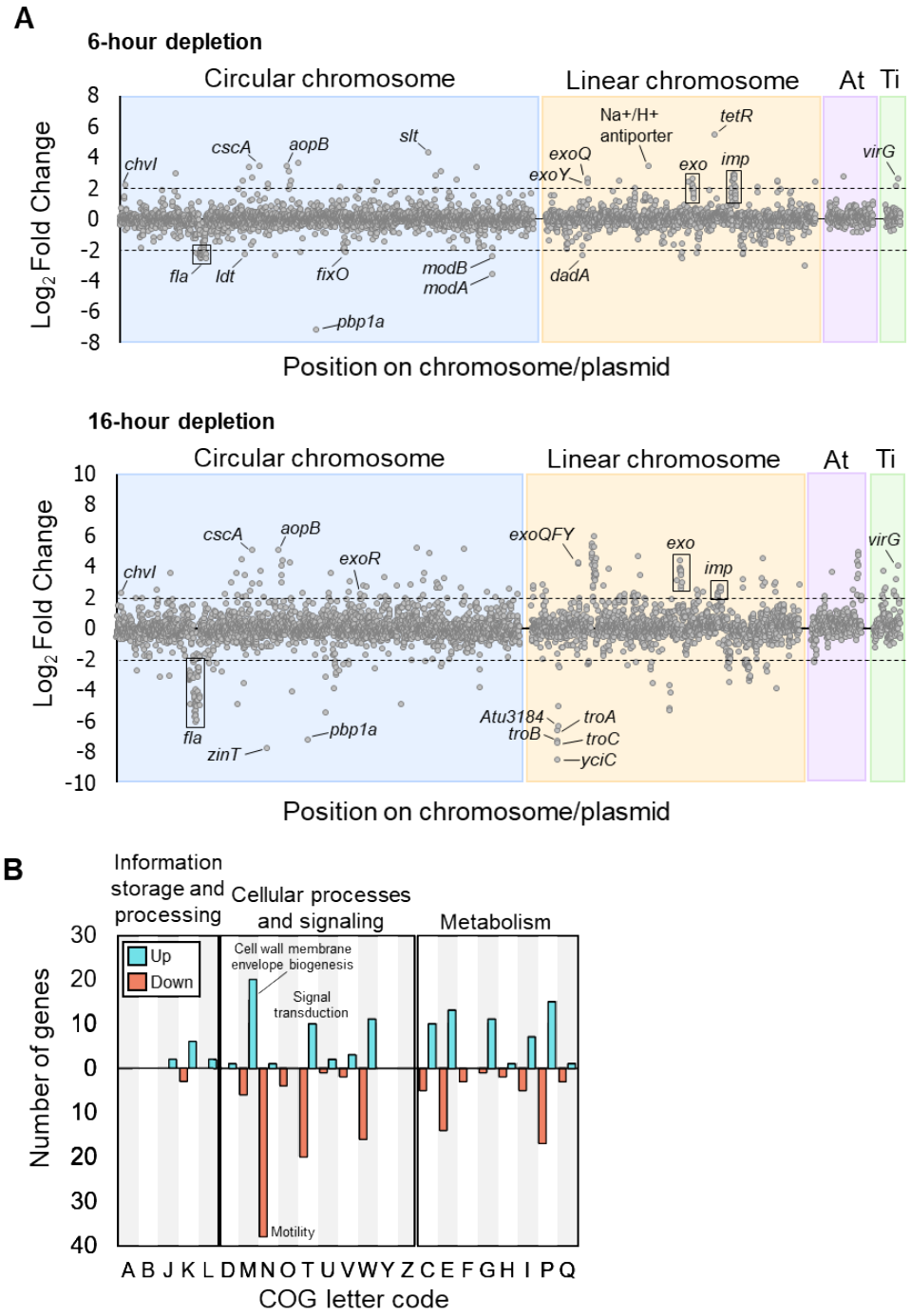

879

880 **Fig 2. Analysis of the PBP1a depletion transcriptomes by RNA-seq.** A. Plots
881 comparing Log2Fold Change of the + PBP1a transcriptome to that of the - PBP1a 6-
882 hour transcriptome and to that of the 16-hour depletion. Gray dots represent a single
883 transcript, and the dotted lines represent +/- 2.0 Log2Fold Change threshold. Plots are
884 delimited by chromosome and mega plasmid. B. COG categorical analysis of the 16-
885 hour depletion of PBP1a. Pink, downregulated; Cyan, upregulated.

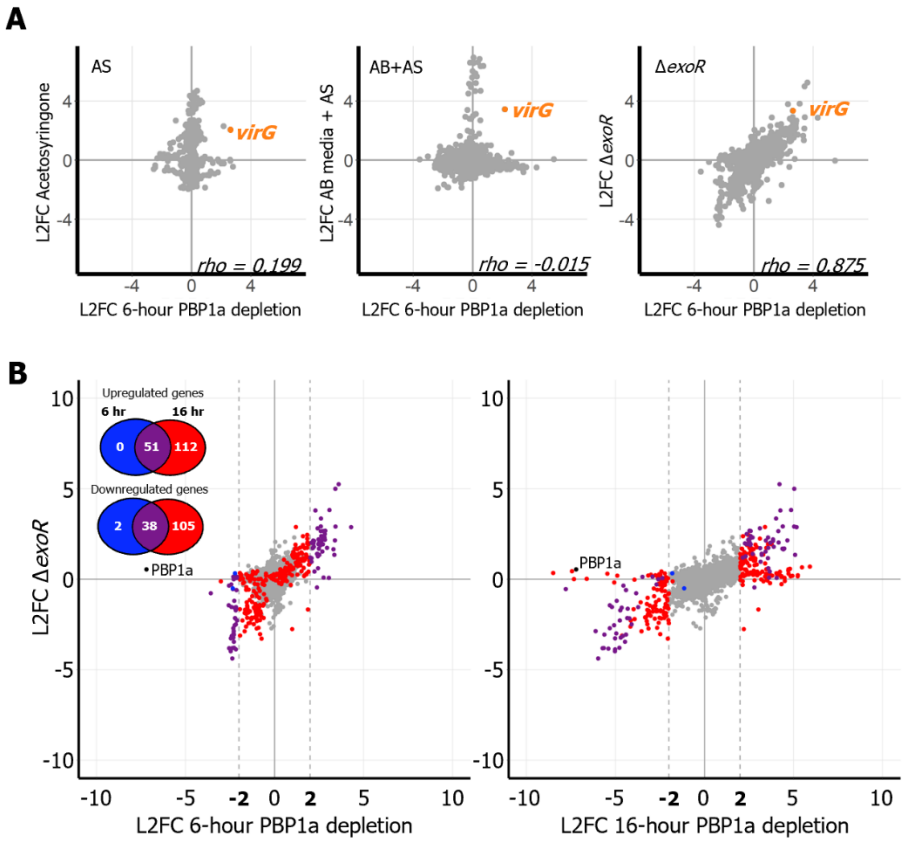

Fig 3. The response to the depletion of PBP1a mimics transcriptional changes associated with host invasion. A. Correlation scatterplots depicting relationships between the log2fold-change (L2FC) values in the 6-hour PBP1a depletion and transcriptomic data sets taken under simulated virulence-inducing conditions (AS and AB+AS) and under simulated host-invading conditions (Δ*exoR*). Each point represents a unique transcript. AS, acetosyrinogone; AB, *Agrobacterium* minimal media; rho, Spearman correlation coefficient. B. Correlation scatterplots comparing L2FC values of transcripts in the Δ*exoR* microarray to either the 6-hour or 16-hour PBP1a depletion. Each transcript is colored according to its change in L2FC values from 6 hours of PBP1a depletion to 16 hours of depletion. Gray, no change; Blue, transcript has |L2FC| > 2.0 in the 6-hour but not in the 16-hour depletion; Red, |L2FC| > 2.0 in the 16-hour but not in the 6-hour depletion; Purple, |L2FC| > 2.0 in both the 6-hour and 16-hour depletion.

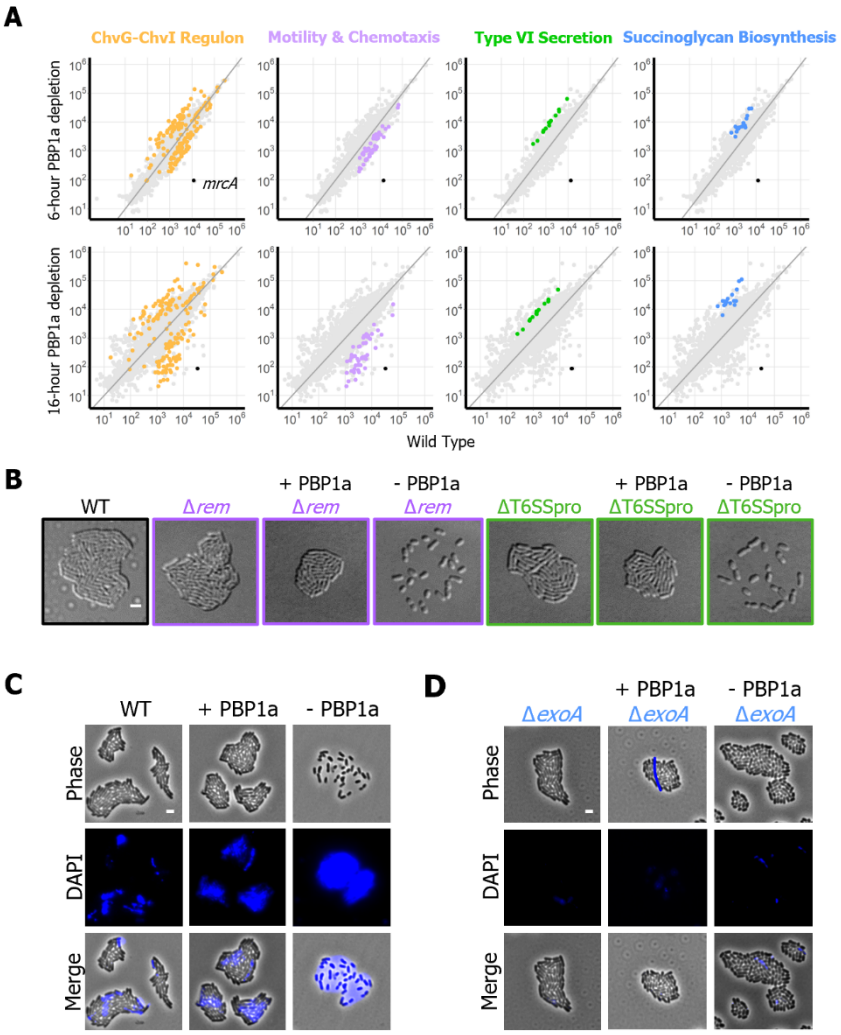

Fig 4. Succinoglycan overproduction is a conserved response to PBP1a depletion and results in failed microcolony formation. A. Scatter plots depicting RPKM values of the 6-hour and 16-hour compared to wild type. Each point represents a unique transcript. Points are colored by category. Gold, ChvG-ChvI regulon; Lavender, Motility and Chemotaxis; Green, Type VI Secretion; Blue, Succinoglycan Biosynthesis; Black, *mrcA* (encoding PBP1a). B. Micrographs of wild type, Δ*rem*, PBP1a replete Δ*rem*, PBP1a depleted Δ*rem*, ΔT6SSpro, PBP1a replete ΔT6SSpro, and PBP1a depleted ΔT6SSpro. Each strain was grown to exponential phase, spotted on a 1% ATGN agar pad containing 1mM IPTG if inducing *mrcA*, allowed to grow for 16 hours, and imaged by DIC microscopy. The scale bar depicts 2μm. C. Micrographs of wild type, and PBP1a depletion with or without IPTG inducer. Each strain was grown to exponential phase and spotted on a 1% ATGN agar pad containing 25μg/mL calcofluor white and 1mM IPTG if inducing *mrcA*. Each was allowed to grow for 16 hours and imaged by phase microscopy with and without the DAPI filter for visualizing calcofluor-stained succinoglycan. D. Micrographs of Δ*exoA* and PBP1a depletion Δ*exoA*, with or without IPTG inducer. Strains were grown and imaged as described for panel C.

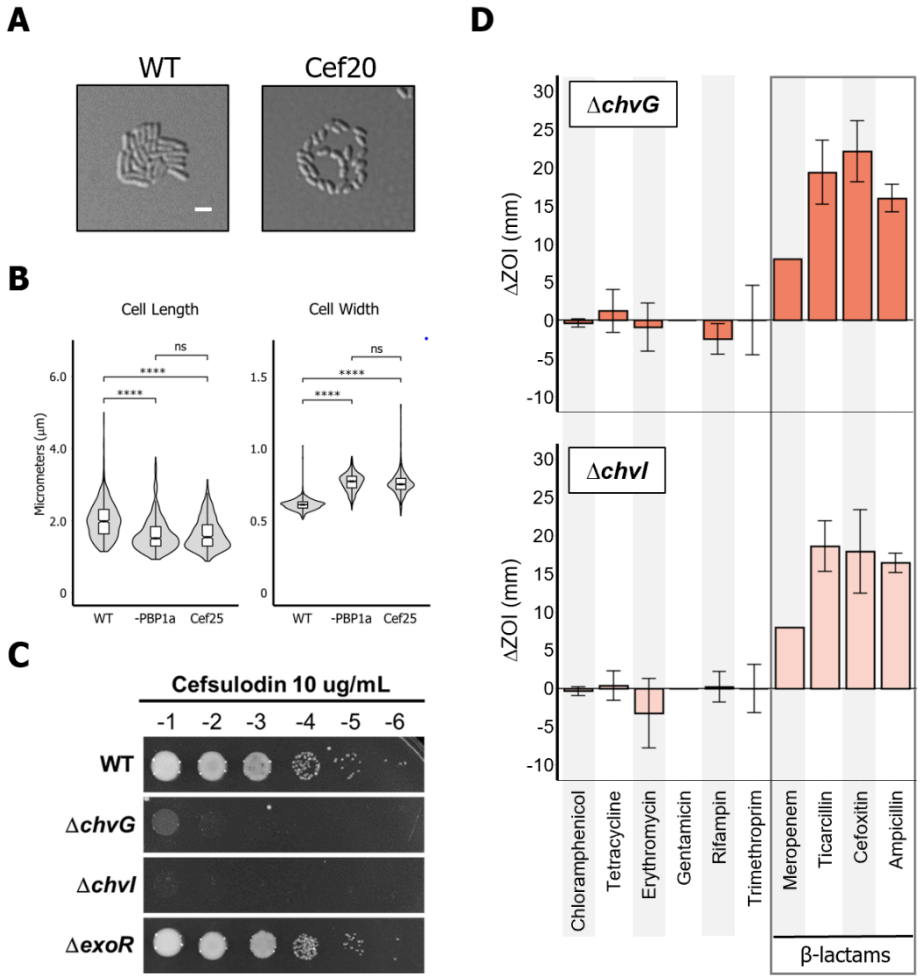

Fig 5. The ChvG-ChvI TCS is conditionally essential under treatment with β-lactam antibiotics. A. Micrographs of untreated and cefsulodin-treated cells. Wild-type cells were grown to exponential phase, spotted on a 1% ATGN agar pad with or without 20 µg/mL cefsulodin and allowed to grow for 16 hours. Each strain was imaged by DIC microscopy. B. Box plots comparing cell length and width between wild-type, PBP1a-depleted, and cefsulodin-treated cells. ns, not significant; ****, $p < 0.00005$. C. Cell viability of each wild type, Δ*chvG,* Δ*chvI,* and Δ*exoR* spotted on an ATGN agar plate containing 10 µg/mL of cefsulodin. Ten-fold serial dilutions are indicated. D. Graph depicting the change in zone of inhibition from wildtype in Δ*chvG* and Δ*chvI* against ten different antibiotic disks. Error bars represent +/- 1 standard deviation from the mean.

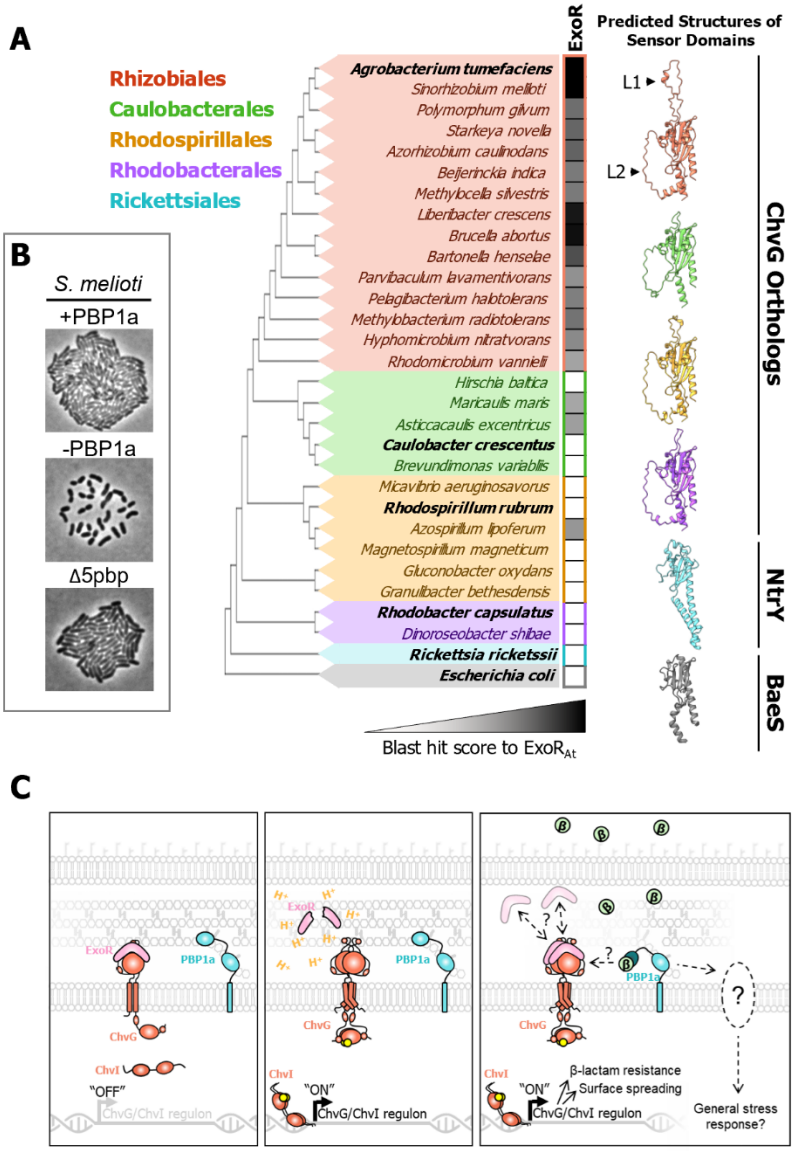

Fig 6. Conservation constraints of ExoR suggest conserved ChvG-ChvI response is independent of ExoR. A. Maximum parsimony tree constructed using MUSCLE sequence alignment [60] on the periplasmic regions of ChvG orthologs. In clades that don't have a ChvG ortholog, the protein with the highest sequence similarity to ChvG was used instead. Conservation of ExoR was calculated using blast max scores from top hits when protein blasting [59] ExoR from *Agrobacterium tumefaciens* against each species in the tree. Phyre2 predicted structures of periplasmic domains of ChvG orthologs from representatives (bold) in each genus are shown. Conserved structural loops are denoted as L1 and L2. B. Micrographs of *Sinorhizobium meliloti* Rm2011 PBP1a replete, PBP1a depleted, and a strain with deletions of genes encoding all other high molecular weight PBPs (Δ5pbp). Each strain was grown to exponential phase, spotted on a 1% TY agar pad containing 1mM IPTG if inducing *mrcA*, allowed to grow for 16 hours, and imaged with phase microscopy. C. Working model of activation of ChvG-ChvI in *A. tumefaciens.* H^+, free proton representing an acidic environment; β, β-lactam antibiotic.